

Double Machine Learning for Estimating Time-Varying Delayed and Instantaneous Effects Using Digital Phenotypes

Xingche Guo

Department of Statistics, University of Connecticut

Zexi Cai

Department of Biostatistics, Columbia University

Yuanjia Wang

Departments of Biostatistics and Psychiatry, Columbia University

Donglin Zeng

Department of Biostatistics, University of Michigan

Abstract

Mobile health (mHealth) leverages digital technologies, such as mobile phones, to capture objective, frequent, and real-world digital phenotypes from individuals, enabling the delivery of tailored interventions to accommodate substantial between-subject and temporal heterogeneity. However, evaluating heterogeneous treatment effects from digital phenotype data is challenging due to the dynamic nature of treatments and the presence of delayed effects that extend beyond immediate responses. Additionally, modeling observational data is complicated by confounding factors. To address these challenges, we propose a double machine learning (DML) method designed to estimate both time-varying instantaneous and delayed treatment effects using digital phenotypes. Our approach uses a sequential procedure to estimate the treatment effects based on a DML estimator to ensure Neyman orthogonality. We establish the asymptotic normality of the proposed estimator. Extensive simulation studies validate the finite-sample performance of our approach, demonstrating the advantages of DML and the decomposition of treatment effects. We apply our method to an mHealth study on Parkinson's disease (PD), where we find that the treatment is significantly more effective for younger PD patients and maintains greater stability over time for individuals with low motor fluctuations. These findings demonstrate the utility of our proposed method in advancing precision medicine in mHealth studies.

Keywords: Dynamic treatment; Heterogeneous treatment effects; Intensive longitudinal data; Mobile health; Neyman orthogonality

1 Introduction

The rapid advancement of mobile health (mHealth) technologies holds promise to revolutionize healthcare through the development of digital phenotypes, which are health-related data collected from interactions with digital technologies, including smartphones and wearable sensors. Extending beyond traditional clinical measures, digital phenotypes can provide comprehensive, real-time information on the manifestations and management of illness (Jain et al., 2015). This innovation is relevant in addressing the challenges posed by chronic neurological disorders, such as Parkinson’s disease (PD), Alzheimer’s disease (AD), and dystonia, where access to adequate neurological care remains a major challenge (Willis et al., 2011). One example of using digital phenotypes to study neurological disorders is the Mobile Parkinson’s Observatory for Worldwide Evidence-based Research (mPower, Bot et al., 2016). In this study, researchers remotely collected digital information on daily symptom assessments (e.g., movement, cognition, and voice) from PD patients via smartphones. Another mHealth example is to use wearable devices in cardiac care by continuously monitoring heart rhythms to detect arrhythmia or predict heart failure (Alugubelli et al., 2022; Bhaladak et al., 2024). Since digital phenotypes enable continuous, real-time health monitoring and assessments, mobile interventions have been developed in a range of applications. For example, mobile platforms are designed for diabetes self-management (Wu et al., 2017), including text messaging and telemedicine to support patient care. Behavioral health interventions, such as self-guided cognitive behavioral therapy (CBT) delivered via mobile phones, have also been shown to effectively treat anxiety and depression (Martinengo et al., 2021).

One key advantage of mHealth interventions is their flexibility and adaptivity to different individuals and adaptation over time for the same individual. This feature is im-

portant given the considerable heterogeneity among patients and the time-varying nature of heterogeneous treatment effects (HTEs). Patient characteristics, including age and comorbidities, as well as time-specific factors such as real-time health states (e.g., symptom fluctuations, stress levels), can significantly influence responses to interventions. In addition, variability in adherence, engagement, and contextual factors, including environment, social interactions, and timing of delivery, further contribute to heterogeneity. For instance, a behavioral intervention may be more effective when delivered during periods of stability than high stress. In the motivating mPower study, patients received long-term dopaminomimetic therapy (e.g., levodopa) to manage their daily motor symptoms. It is important to estimate the dynamic effects of interventions using digital phenotype data in mHealth studies to improve care. For example, by capturing these dynamics, adaptive intervention strategies can be developed to tailor treatments to individual patients, improving efficacy and patient engagement. Furthermore, exploring the temporal patterns in treatment effects also facilitates better intervention delivery based on patient's needs, thus advancing personalized medicine and the success of mHealth interventions.

For many mHealth applications, dynamic HTE estimation needs to account for delayed or lagged effects, where the benefits of an intervention persist or become apparent only after a certain period post-administration. For PD, while levodopa treatment provides immediate relief of motor symptoms by replenishing dopamine levels, its effects on motor learning may take weeks to months to manifest. For instance, physical rehabilitation paired with levodopa treatment may result in cumulative motor function improvements over time due to enhanced neuroplasticity (Keus et al., 2014). Prolonged levodopa use is associated with the development of motor complications such as dyskinesias (involuntary movements), which often appear after several years of treatment (Obeso et al., 2000) as delayed adverse

effects. Similarly, stress management interventions may show delayed effects as patients gradually learn and practice coping strategies (Hofmann et al., 2010). Thus, mindfulness or cognitive-behavioral therapy mobile apps might not yield noticeable improvements in stress levels until weeks of consistent use. These examples suggest that it is important to develop methods to account for delayed effects in dynamic HTE estimation.

Methods have been developed to estimate treatment effects using longitudinal or time-series data. In particular, the difference-in-differences (DiD) method is a widely used tool to draw causal inferences under the parallel trends assumption, i.e., in the absence of treatment, treated and untreated groups would have similar trends; see the review in Callaway and Sant'Anna (2021). Various extensions have been proposed to relax this assumption by weighting different subjects and time periods, including synthetic control (Abadie et al., 2010) and its variations (e.g., Arkhangelsky et al., 2021). However, these approaches do not handle delayed treatment effects. Towards this end, Sun and Abraham (2021) modeled delayed treatment effects using a parametric dynamic treatment effect model in staggered treatment adoption settings, providing cohort-specific average treatment effects for each cohort and relative time period. Hatamyar et al. (2023) proposed a Machine Learning Difference-in-Differences (MLDID) method for time-varying conditional average treatment effects on the treated, accounting for dynamic heterogeneity across subpopulations and over time. Lewis and Syrgkanis (2021) extended the G-estimation framework for structural nested mean models to dynamic treatment regimes and proposed robust estimation of dynamic effects in high-dimensional settings using double machine learning (Chernozhukov et al., 2018). Loh and Ren (2023) presented a G-estimation to assess the causal effects of time-varying treatments in longitudinal studies by appropriately adjusting for time-dependent confounders. However, none of these aforementioned methods separate imme-

diate treatment effect from delayed effect due to prior treatment periods.

In this paper, we extend a double machine learning (DML) method (Chernozhukov et al., 2018) to estimate time-varying delayed and instantaneous effects using digital phenotype data to ensure the robustness of treatment effect estimates to the misspecification of nuisance parameters (e.g., propensity scores and outcome models). DML methods have been used to estimate HTEs for single time-point settings, such as causal forests (Wager and Athey, 2018) and R-Learner (Nie and Wager, 2021). In our work, we decompose the treatment effect on the outcome at each time point into four distinct components: the baseline effect, the delayed effect, the instantaneous effect (when treated), and the additional prognostic effect. This decomposition leads to a more accurate estimation of HTEs to capture how the treatment effect manifests over time. We use machine learning (ML) models, such as random forests and gradient boosting machines, to estimate both the baseline and prognostic effects, ensuring flexibility and robustness in capturing complex relationships. The time-varying instantaneous treatment effects are modeled through sequential updates, allowing the method to adapt to changes over time. A flexible framework is adopted to capture the delayed effects, accommodating various temporal dependencies. To address confounding in mHealth studies, we also model the propensity scores using ML models. Finally, we apply the DML framework to ensure unbiased estimation of the treatment effects, leveraging Neyman orthogonalization to control for confounding factors and protect against model misspecification. This methodology enhances the accuracy and reliability of effect estimates in dynamic treatment settings, particularly when utilizing rich digital phenotype data.

The remainder of the article is organized as follows. Section 2 introduces the proposed model for estimating time-varying delayed and instantaneous effects. Section 3 outlines

the DML method for estimation and demonstrates that the proposed estimating equation satisfies the Neyman orthogonality condition. Section 4 presents the asymptotic theory and the statistical inference procedure. Section 5 provides the results of our simulation studies, while Section 6 applies the method to analyze digital phenotype data from an mHealth study. Finally, Section 7 summarizes our approach and main findings and discusses potential extensions for future research. The Appendix contains proofs of the main theoretical results.

2 Model

We propose a general framework for estimating time-varying heterogeneous treatment effects (tv-HTEs) in mobile health studies, where treatments are administered at each discrete time $t = 1, 2, \dots, T$ and T is the maximum number of time points. At time t , each subject has a single outcome measurement, which may be recorded either while the subject is under treatment (e.g., a subject has just completed a session of CBT delivered via a mobile phone or just taken a levodopa medication) or when they are not receiving treatment. Let $Y_{it}^{(1)}$ denote the potential outcome for subject i when the treatment is given at time t , and $Y_{it}^{(0)}$ be the potential outcome when the treatment is not administered at t . Let Z_i denote time-invariant baseline covariates (e.g., race, gender, age). We further denote A_{it} as the treatment status at time t (1: treated; 0, not treated), X_{it} as pre-specified time-dependent effect modifiers of interest for studying HTEs, and U_{it} as additional time-dependent prognostic factors and auxiliary covariates (e.g., measurement gap times), which are also predictive of potential outcomes but are not effect modifiers. Note that U_{it} has no overlap with X_{it} . Here, we assume that all covariates are observed at all time points t .

To model the delayed treatment effects, we assume that along with other prognostic

factors, the treatment effects from the past contribute additively to the potential outcome at time t before any treatment administration. Specifically, let \mathcal{H}_{it} include Z_i , treatment history ($A_{is}, s = 1, \dots, t-1$) indicating treatment status at each time point, and covariate history up to time t , $(X_{is}, U_{is}, s = 1, \dots, t)$. We assume that for $t > 1$,

$$E(Y_{it}^{(0)} \mid \mathcal{H}_{it}) = E(Y_{i1}^{(0)} \mid Z_i) + \sum_{s=1}^{t-1} w_{s,t-s} A_{is} E(Y_{is}^{(1)} - Y_{is}^{(0)} \mid \mathcal{H}_{is}) + \delta_{0t}(U_{it}, X_{it}). \quad (1)$$

Here, the first term on the right-hand side of (1) is the baseline effect at $t = 1$. The second term is the delayed effects from the past $t - 1$ treatment episodes on the current potential outcome prior to the administration of another episode of treatment, and $w_{s,t-s} \in [0, 1]$ is the delayed discounting factor representing the diminished impact of previous treatments over time. The third term is assumed to be fully unknown, and it captures the additional prognostic effect at current time $t > 1$, such as changes in disease prognosis from baseline to the present, with $\delta_{01}(\cdot) \equiv 0$. Therefore, model (1) assumes that the expected outcome at time t , if treatment is not administered, is an additive function of the baseline outcome, the cumulative treatment effects from the past, and may also be affected by the time-varying features. When $w_{s,t-s} \equiv 0$, it indicates the absence of delayed treatment effects, and the short-term treatment effect completely diminishes before the next treatment episode (Xu et al., 2023) so that the patient's outcome returns to the pre-treatment level. Conversely, when $w_{s,t-s} \equiv 1$, it indicates that the treatment effect is cumulative with no decay. In our applications, we assume $w_{s,t-s} := \gamma^{t-s}$ for $\gamma \in (0, 1)$, implying that the treatment effect decays exponentially with a lag of $t - s$. Next, to model the instantaneous treatment effect and account for possible HTEs, we assume the difference in potential outcomes to be a

linear function of the current effect modifiers X_{it} and Z_i :

$$E(Y_{it}^{(1)} - Y_{it}^{(0)} \mid \mathcal{H}_{it}) = \beta_{0t}^\top \tilde{X}_{it}, \quad (2)$$

where $\tilde{X}_{it} = (1, Z_i^\top, X_{it}^\top)^\top$.

Our structural models can be displayed in the following Figure 1, which shows the relationships between baseline factors, time-varying prognostic factors, treatment modifiers, and potential outcomes based on model (1). The diagram shows the dynamic nature of treatment effects, distinguishing between instantaneous effects and delayed effects propagating to later outcomes. This structure allows the model to account for the cumulative prognostic effects over time, providing a framework to estimate time-varying HTEs. To improve readability, certain components of the model, including effects on potential outcomes $Y_{it}^{(1)}$, treatment modification effect, and confounders (e.g., covariate history), are not shown on the diagram.

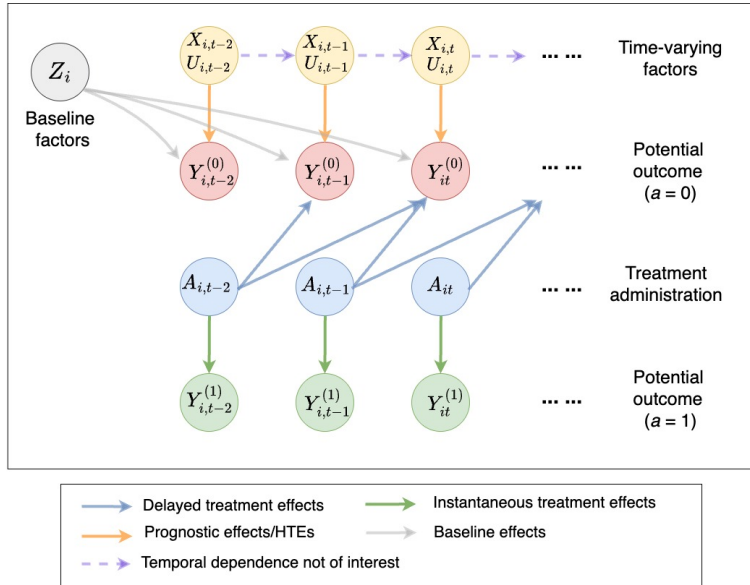


Figure 1: Schematic diagram illustrating the decomposition of dynamic treatment effects into instantaneous and delayed effects. To improve readability, treatment effect modification and confounding are not shown on the diagram.

Observed data consist of the covariate history, response outcome measurements, and treatment status at time $t = 1, 2, \dots, T$ from n i.i.d subjects. We assume the observed data as follows:

$$(Z_i, X_{it}, U_{it}, A_{it}, Y_{it}, t = 1, \dots, T), \quad i = 1, \dots, n.$$

To infer both dynamic and instantaneous HTEs, we need two additional assumptions, which correspond to sequential ignorability and Stable Unit Treatment Value Assumption (SUTVA) that are commonly assumed in causal inference (e.g., Ding, 2024). That is, we assume $A_{it} \perp Y_{it}^{(a)} \mid \mathcal{H}_{it}$, and Y_{it} is the potential outcome corresponding to the treatment status for time t .

3 Estimation and Inference

We describe the estimation procedures for robustly estimating tv-HTEs in a sequential fashion using the DML. For simplicity, we denote $Y_{it} = Y_{it}^{(A_{it})}$. We begin by estimating the baseline effect, $g_0(Z_i) = E(Y_{i1}^{(0)} \mid Z_i)$, through minimizing:

$$\ell_1(g) = \frac{1}{n} \sum_{i=1}^n I(A_{i1} = 0) \{Y_{i1} - g(Z_i)\}^2,$$

where $g(\cdot)$ can be approximated using nonparametric or machine learning methods such as splines or random forest. We can show that the expectation of the score function of $\ell_1(g)$ at g_0 is equal to 0. Therefore, this method provides an asymptotically unbiased estimator as n goes to infinity. Next, we fit a propensity score model using machine learning methods such as random forest, gradient boosting, or neural networks for

$$\pi_{0t}(\mathcal{H}_{it}) = E(A_{it} \mid \mathcal{H}_{it}), \quad t = 1, \dots, T.$$

We denote the estimates for g_0 and π_{0t} as \hat{g} and $\hat{\pi}_t$, respectively.

To estimate tv-HTEs, we note that the potential outcome $Y_{it}^{(0)}$ in model (1) depends on the unknown treatment effects from prior time points, and thus the estimation needs to proceed sequentially over time. We first assume that the delayed discounting factor γ is known; the case where γ must be estimated will be addressed at the end of this section. Suppose that at time $t > 1$, we have already obtained estimates $\hat{\beta}_1, \dots, \hat{\beta}_{t-1}$. At time t , the estimation proceeds in two steps:

Step 1. Using all observations with $A_{it} = 0$ to estimate $\delta_{0t}(\cdot)$ given \mathcal{H}_{it} by minimizing

$$\ell_t(\delta_t) = \frac{1}{n} \sum_{i=1}^n I(A_{it} = 0) \left\{ Y_{it} - h_t \left(\mathcal{H}_{it}; \hat{g}, \delta_t, \{\hat{\beta}_s\}_{s=1}^{t-1} \right) \right\}^2,$$

where h_t is given in Step 2. Let $\hat{\delta}_t$ be the estimate from this step.

Step 2. Estimate the tv-HTE β_{0t} using DML: We solve for β_{0t} using residuals of outcomes under treatment and ‘centered treatment indicators’:

$$\frac{1}{n} \sum_{i=1}^n \left\{ Y_{it} - A_{it} \beta_t^\top \tilde{X}_{it} - \hat{h}_t(\mathcal{H}_{it}) \right\} \{A_{it} - \hat{\pi}_t(\mathcal{H}_{it})\} \tilde{X}_{it} = 0, \quad (3)$$

where $\hat{h}_t(\mathcal{H}_{it}) = h_t \left(\mathcal{H}_{it}; \hat{g}, \hat{\delta}_t, \{\hat{\beta}_s\}_{s=1}^{t-1} \right)$ with

$$h_t \left(\mathcal{H}_{it}; g_0, \delta_{0t}, \{\beta_{0s}\}_{s=1}^{t-1} \right) = g_0(Z_i) + I(t > 1) \left\{ \sum_{s=1}^{t-1} A_{is} w_{s,t-s} \beta_{0s}^\top \tilde{X}_{is} + \delta_{0t}(U_{it}, X_{it}) \right\}.$$

If there are high-dimensional effect modifiers and we are only interested in the effect of a few modifiers, we can perform variable selection and estimate the tv-HTE for the modifiers selected using (3).

In the following, we provide an intuitive explanation of why the proposed method

should yield consistent estimators. Most importantly, we show that (3) satisfies the Neyman orthogonality property. This property is crucial to ensure $\hat{\beta}_t$ to be consistent and asymptotically Gaussian while allowing the estimators for $\pi_{0t}(\cdot)$ and $h_{0t}(\cdot)$ to have relatively slower convergence rates (see Section 4 for more details). Denote $\{A_t, Y_t, \mathcal{H}_t\}_{t=1}^T$ as a copy of the digital phenotype data. Define

$$S_t(\beta_t, \eta_t) = \left\{ Y_t - A_t \beta_t^\top \tilde{X}_t - h_t(\mathcal{H}_t) \right\} \left\{ A_t - \pi_t(\mathcal{H}_t) \right\} \tilde{X}_t, \quad (4)$$

where $\eta_t = (h_t, \pi_t)^\top$. The score function (3) can be expressed by $\Psi_t(\beta_t, \eta_t) = \mathbb{P}_n S_t(\beta_t, \eta_t)$, where \mathbb{P}_n is the empirical measure. According to model (1)-(2), rewrite

$$Y_t^{(A_t)} = A_t \beta_{0t}^\top \tilde{X}_t + h_{0t}(\mathcal{H}_t) + W_t^{(A_t)}, \quad (5)$$

where $W_t^{(a)}$ is disturbance for $a = 0, 1$ and $E(W_t^{(a)} \mid \mathcal{H}_{it}) = 0$. For simplicity, we denote $W_t = W_t^{(A_t)}$. Define $V_t = A_t - \pi_{0t}(\mathcal{H}_t)$, according to (4),

$$S_t(\beta_{0t}, \eta_t) = \left\{ W_t + \Delta h_t(\mathcal{H}_t) \right\} \left\{ V_t + \Delta \pi_t(\mathcal{H}_t) \right\} \tilde{X}_t, \quad (6)$$

where $\Delta h_t = h_{0t} - h_t$, $\Delta \pi_t = \pi_{0t} - \pi_t$. Thus, we have $S_t(\beta_{0t}, \eta_{0t}) = W_t V_t \tilde{X}_t$ and $E[S_t(\beta_{0t}, \eta_{0t})] = 0$. It holds because $E[W_t V_t \mid \mathcal{H}_t] = \pi_{0t}(\mathcal{H}_t)(1 - \pi_{0t}(\mathcal{H}_t))E[W_t^{(1)} - W_t^{(0)} \mid \mathcal{H}_t] = 0$. Next, we introduce a small bias $\rho \Delta \eta_t$ around the true value η_{0t} , and take the derivative of $E[S_t(\beta_{0t}, \eta_{0t} + \rho \Delta \eta_t)]$ with respect to ρ , we have

$$\lim_{\rho \rightarrow 0} \frac{\partial}{\partial \rho} E[S_t(\beta_{0t}, \eta_{0t} + \rho \Delta \eta_t)] = E \left[\{V_t \Delta h_t(\mathcal{H}_t) + W_t \Delta \pi_t(\mathcal{H}_t)\} \tilde{X}_t \right] = 0. \quad (7)$$

Equation (7) is referred to as the Neyman orthogonality property. Thus, following Cher-

nozhukov et al. (2018), this property implies that the score function, $S_t(\beta_t, \eta_t)$, is insensitive to small estimation biases in the nonparametric function η_t .

Remark 1. When the delayed discounting factor γ is unknown, we treat it as a tuning parameter. Specifically, the root mean squared error (RMSE) between the true and estimated responses is computed for a given discounting factor γ , denoted as $\mathcal{R}(\gamma)$, and the optimal γ is determined by minimizing $\mathcal{R}(\gamma)$. Alternatively, other criteria, such as the root mean squared percentage error (RMSPE) or cross-validation (CV) scores, can also be used to select γ .

4 Asymptotic Theory

Define $\Psi_t^a(\eta_t) = \mathbb{P}_n A_t \{A_t - \pi_t(\mathcal{H}_t)\} \tilde{X}_t \tilde{X}_t^\top$, $\Psi_t^b(\eta_t) = \mathbb{P}_n \{Y_t - h_t(\mathcal{H}_t)\} \{A_t - \pi_t(\mathcal{H}_t)\} \tilde{X}_t$, where \mathbb{P}_n is the empirical measure (Vaart and Wellner, 1996). Define $\hat{J}_t = \Psi_t^a(\hat{\eta}_t)$. According to (3), $\hat{\beta}_t$ has an explicit form: $\hat{\beta}_t = \hat{J}_t^{-1} \Psi_t^b(\hat{\eta}_t)$. Denote $\mathcal{T} = \{1, 2, \dots, T\}$, assume that \mathcal{T} is a finite set. Assume that the dimension of \tilde{X}_t , d , is finite. We establish the asymptotic conditions under which $n^{1/2}(\hat{\beta}_t - \beta_{0t})$ converges in distribution to a Gaussian limit uniformly for all $t \in \mathcal{T}$. The following conditions are needed for the theorems in this paper.

CONDITION 1. For $t \in \mathcal{T}$, $p_a < \pi_{0t}(\mathcal{H}_t) < 1 - p_a$ for small $p_a > 0$, and $E(W_t^2 | \mathcal{H}_t) < \infty$.

CONDITION 2. Define $\Sigma_t = E[\tilde{X}_t \tilde{X}_t^\top]$, let $\Lambda_{\min}(\cdot)$ and $\Lambda_{\max}(\cdot)$ denote the minimum and maximum eigenvalues for a matrix, then,

$$0 < \sigma_{\min}^2 \leq \inf_{t \in \mathcal{T}} \Lambda_{\min}(\Sigma_t) \leq \sup_{t \in \mathcal{T}} \Lambda_{\max}(\Sigma_t) \leq \sigma_{\max}^2 < \infty.$$

Furthermore, define $H_t = E[(\tilde{X}_t \tilde{X}_t^\top) \otimes (\tilde{X}_t \tilde{X}_t^\top)]$, we have $\sup_{t \in \mathcal{T}} \Lambda_{\max}(H_t) \leq \kappa_{\max}^4 < \infty$.

CONDITION 3. Suppose $\hat{\pi}_t \in \mathcal{F}_\pi$, $\hat{g} \in \mathcal{F}_g$, and $\hat{\delta}_t \in \mathcal{F}_\delta$, where \mathcal{F}_π , \mathcal{F}_g , \mathcal{F}_δ are P -Donsker.

Furthermore, denote $E^* \|f\|^d = \int |f|^d dP_{\mathcal{H}_t^*}$, where \mathcal{H}_t^* is an independent copy of $\{\mathcal{H}_{it}\}_{i=1}^n$.

We assume $E^* \|\widehat{g} - g_0\|^4 = o_p(1)$, $\sup_{t \in \mathcal{T}} E^* \|\widehat{\delta}_t - \delta_{0t}\|^4 = o_p(1)$, $\sup_{t \in \mathcal{T}} E^* \|\widehat{\pi}_t - \pi_{0t}\|^4 = o_p(1)$,

and

$$\sup_{t \in \mathcal{T}} E^* \|(\widehat{\delta}_t - \delta_{0t})(\widehat{\pi}_t - \pi_{0t})\|^2 = o_p(n^{-1}), \quad \sup_{t \in \mathcal{T}} E^* \|(\widehat{g} - g_0)(\widehat{\pi}_t - \pi_{0t})\|^2 = o_p(n^{-1}).$$

Condition 1 ensures the effective sample size at any given time point t , both treated and untreated, is of the same order as the total number of subjects n . Condition 2 imposes regularization constraints on the second and fourth moments of \tilde{X}_t . Condition 2 is mild, as it is readily satisfied by Gaussian random variables. Condition 3 imposes constraints on the model complexity of the machine learning estimators, requires the consistency of the estimates, and specifies the order of the estimation errors. Moreover, by the definition of $h_t(\cdot)$, imposing assumptions on $g(\cdot)$ and $\delta_t(\cdot)$ is equivalent to imposing assumptions on $h_t(\cdot)$. Specifically, for $\widehat{h}_t \in \mathcal{F}_{h_t}$, \mathcal{F}_{h_t} is P -Donsker. Also, $\sup_{t \in \mathcal{T}} E^* \|\widehat{h}_t - h_{0t}\|^4 = o_p(1)$, $\sup_{t \in \mathcal{T}} E^* \|(\widehat{h}_t - h_{0t})(\widehat{\pi}_t - \pi_{0t})\|^2 = o_p(n^{-1})$.

Theorem 1. *Under Conditions 1–3, as $n \rightarrow \infty$, the joint distribution of the tv-HTE estimators has the following asymptotic expression*

$$n^{1/2} (\widehat{\beta} - \beta_0) \xrightarrow{d} N(0, \Gamma_0^{-1} \Psi_0 \Gamma_0^{-1}),$$

where $\widehat{\beta} = (\widehat{\beta}_1^\top, \dots, \widehat{\beta}_T^\top)^\top$, $\beta_0 = (\beta_{01}^\top, \dots, \beta_{0T}^\top)^\top$; $\Gamma_0 = \text{diag}(J_{0t})_{t \in \mathcal{T}}$, $J_{0t} = E[\Psi_t^a(\eta_{0t})]$; $\Psi_0 = (\Omega_{0,tt'})_{t,t' \in \mathcal{T}}$, $\Omega_{0,tt'} = E[S_t(\beta_{0t}, \eta_{0t}) S_{t'}^\top(\beta_{0t'}, \eta_{0t'})]$.

The proof of the theorem is in the Web Appendix A. By the definition of $\Psi_t^a(\eta_{0t})$, we

can express J_{0t} by

$$J_{0t} = E \left[A_t V_t \tilde{X}_t \tilde{X}_t^\top \right] = E \left[\pi_{0t}(\mathcal{H}_t) (1 - \pi_{0t}(\mathcal{H}_t)) \tilde{X}_t \tilde{X}_t^\top \right].$$

Under Conditions 1 and 2, J_{0t} is positive definite with eigenvalues bounded away from zero and infinity. Meanwhile, $\Omega_{0,tt} = E(W_t^2 V_t^2 \tilde{X}_t \tilde{X}_t^\top)$, and it can similarly be shown that $\Omega_{0,tt}$ is positive definite with bounded eigenvalues. This ensures that the covariance of the limiting Gaussian distribution is finite, allowing us to conduct statistical inference as follows: Here, $\widehat{\Gamma} = \text{diag}(\widehat{J}_t)_{t \in \mathcal{T}}$, $\widehat{J}_t = \Psi_t^a(\widehat{\eta}_t)$, $\widehat{\Psi} = (\widehat{\Omega}_{tt'})_{t,t' \in \mathcal{T}}$, $\widehat{\Omega}_{tt'} = \mathbb{P}_n[S_t(\widehat{\beta}_t, \widehat{\eta}_t) S_{t'}^\top(\widehat{\beta}_{t'}, \widehat{\eta}_{t'})]$. We can consistently estimate the variance-covariance matrix for $n^{1/2}(\widehat{\beta} - \beta_0)$ as $\widehat{\Sigma} = \widehat{\Gamma} \widehat{\Psi}^{-1} \widehat{\Gamma}$. Thus, we construct the $(1 - \alpha) \times 100\%$ confidence intervals for the k -th entry of β_{0t} , denoted as $\beta_{0t}^{(k)}$, by:

$$\widehat{\beta}_t^{(k)} \pm z_{1-\alpha/2} \sqrt{n^{-1} \left(\widehat{J}_t^{-1} \widehat{\Omega}_{tt} \widehat{J}_t^{-1} \right)_{(k,k)}}, \quad (8)$$

where $z_{1-\alpha/2}$ denotes the $1 - \alpha/2$ quantile of the standard normal distribution. In addition, to test if there are overall excursion effects (i.e., $\beta_{0t} = 0$ for all $t \in \mathcal{T}$), one can construct an overall test based on Hotelling's T^2 test statistic, $n \widehat{\beta}^\top (\widehat{\Gamma} \widehat{\Psi}^{-1} \widehat{\Gamma})^{-1} \widehat{\beta}$, which is approximately χ_{Td}^2 distributed for large n .

Remark 2. Our proposed framework provides the estimated sequence for β_t , denoted by $\widehat{\beta}_t$. In some practices, one may be interested in a parametric model for β_t by assuming $\beta_t = f(t; \theta)$, for example, f is a linear or quadratic function for β_t . With the estimated $\widehat{\beta}_t$ and their covariance matrix $\widehat{\Sigma}$, we can estimate θ by minimizing $(\widehat{\beta}_1, \dots, \widehat{\beta}_T) \widehat{\Sigma}^{-1} (\widehat{\beta}_1, \dots, \widehat{\beta})^T$ and the resulting estimator for θ can be easily shown to follow an asymptotically normal distribution using the asymptotic properties for $\widehat{\beta}_t$ as given in this section.

Finally, we provide an asymptotic result when T is large, which is typical in mHealth applications. To this end, we assume that the true value for β_t arises from a function in $[0, 1]$, denoted as $\xi_0(\cdot)$, such that $\beta_{0t} = \xi_0(t/T)$. Correspondingly, we define a stochastic process, $\widehat{\xi}(\cdot)$, such that $\widehat{\xi}(t/T) = \widehat{\beta}_t$, and for any $s \in [(t-1)/T, t/T]$, $\widehat{\xi}(s) = \widehat{\beta}_t$. In other words, $\widehat{\xi}(\cdot)$ is a piecewise stochastic process in $[0, 1]$. Similarly, let $\widetilde{\Gamma}(s)$ be a stochastic function $[0, 1]$ such that $\widetilde{\Gamma}(t/T) = J_t^{-1}S_t(\beta_{0t}, \eta_{0t})$, and it is the same between $(t-1)/T$ and t/T . In addition, we assume that A_t, Y_t and \widetilde{X}_t are the realization of some random processes in $[0, 1]$ at time t/T , and that these random processes have bounded total variations with probability one. The following gives the asymptotic property for $\widehat{\xi}(\cdot)$.

Theorem 2. *In addition to Conditions 1–3, we assume that ξ_0 is continuously differentiable in $[0, 1]$ and that there exists a continuous bivariate function, $\widetilde{\Sigma}_0$, such that $\text{Cov}(\widetilde{\Gamma}(s), \widetilde{\Gamma}(s'))$ converges to $\widetilde{\Sigma}_0(s, s')$ for any $s, s' \in [0, 1]$. Assume $\sqrt{n}/T \rightarrow 0$. Then $\sqrt{n}(\widehat{\xi}(s) - \xi_0(s))$ weakly converges to a tight Gaussian process with mean zero and covariance function $\widetilde{\Sigma}_0(s, s')$ in $l^\infty[0, 1]$.*

This theorem gives the uniformly weak convergence for the piecewise-constant process given by $\widehat{\beta}_t$ when the number of time points is large. One useful application based on this theorem is that we can construct a confidence band or perform global testing over all the time points.

5 Simulations

We conducted extensive simulation studies to evaluate the finite-sample performance of the proposed method. Baseline covariates $Z_i = (Z_{i1}, Z_{i2})$ were generated with each sampled independently from a standard normal distribution. For the time-varying covariates, $X_{it} =$

$(X_{i1t}, X_{i2k})^\top$, we used the following generative model to simulate fluctuating trajectories to mimic subjects' daily physical activities: for $q = 1, 2$

$$X_{iqt} = \sqrt{2} \sum_{k=1}^K \xi_{iqk} \sqrt{\nu_k} \cos(k\pi t) + \epsilon_{iqt}, \quad (9)$$

where $\xi_{iqk} \sim$ i.i.d. $N(0, 1)$ represents the functional principal scores, and $\epsilon_{iqt} \sim$ i.i.d. $N(0, \sigma_\epsilon^2)$ is the noise term. In our simulations, we set $\sigma_\epsilon = 0.75$, $\nu_k = 0.3e^{-k/8}$, and $K = 30$. Assume all subjects have the same trial length $T = 100$, and let $\rho = t/T$ represent the scaled time. We define the tv-HTEs as $\beta_{0t} = (\beta_{0t}^{(0)}, \beta_{0t}^{(z)}, \beta_{0t}^{(x)})$. The intercept term is given by $\beta_{0t}^{(0)} = -0.3(1 - \rho/2)$; the tv-HTEs for the baseline covariates are given by $\beta_{0t}^{(z)} = (0.05, -0.05)$; the tv-HTEs for the time-varying covariates are given by $\beta_{0t}^{(x)} = (0.05 + 0.1\rho^2, -0.05 - 0.1\rho^2)$. In this simulation, we assume that the prognostic factors $U_{it} = (U_{i1t}, \dots, U_{iRt})^\top$ represent distinct physical activities, separate from the time-varying modifiers X_{it} . Each element of U_{it} is generated using equation (9). Consequently, the components of U_{it} are independent of one another, and U_{it} is independent of X_{it} . We considered the delay factors $\gamma \in \{0.3, 0.7\}$. To mimic the complexities encountered in real-world studies, our simulation framework includes a missing data component. Specifically, each observation is assumed to be missing with probability 0.3. The proposed approach remains valid under the missing at random assumption.

We considered two data-generating scenarios:

Case I: In this scenario, we assumed the presence of numerous irrelevant prognostic factors, setting the number of prognostic factors to be 8. We defined $\mu_{it} = X_{i1t} + U_{i1t} + U_{i2t}$, which influenced both the propensity score and the prognostic function, by assuming the probability of treatment, i.e., $A_{it} = 1$, to be given by $\pi_{0t}(\mathcal{H}_{it}) = 1/(1 + \exp(-\frac{1}{2}\mu_{it}))$, and the prognostic function to be $\delta_{0t}(X_{it}, U_{it}) = 0.05(\mu_{it} + N(0, 1))$. The baseline outcome was

specified as $g_0(Z_i) = -1.5 + 0.1(Z_{i1} + Z_{i2}) + N(0, 0.2^2)$.

Case II: In this scenario, we considered a more nonlinear relationship for both the propensity score and prognostic function. Here, we set the number of prognostic factors to be 2, $\nu_{it} = 2 \cdot I(\{X_{i1t} > 1\} \cup \{U_{i1t} > 0.2\}) - 1$. The probability of $A_{it} = 1$ was then given by $\pi_{0t}(\mathcal{H}_{it}) = 1/(1 + \exp(\nu_{it}))$, and the prognostic function was defined as $\delta_{0t}(X_{it}, U_{it}) = 0.15\nu_{it} + N(0, 0.02^2)$. The baseline expected outcome was specified as $g_0(Z_i) = -1.5 + 0.5I(|Z_{i1}| > 0.5) + N(0, 0.2^2)$.

Table 1: Summary of the estimated tv-HTEs across 500 simulations for Case I.

tv-HTE	Method	n = 200												n = 500											
		$\gamma = 0.3$				$\gamma = 0.7$				$\gamma = 0.3$				$\gamma = 0.7$											
		Bias	SD	SE	CP	Bias	SD	SE	CP	Bias	SD	SE	CP												
Intercept	Proposed (known)	-0.8	5.8	5.4	92.6	-0.7	5.8	5.4	92.6	-0.6	3.4	3.3	93.9	-0.6	3.4	3.3	94.0	-0.6	3.4	3.3	94.0	-0.6	3.4	3.3	94.0
	Proposed (estimated)	-0.8	5.7	5.4	92.6	-0.7	5.8	5.4	92.6	-0.6	3.4	3.3	93.9	-0.6	3.4	3.3	94.0	-0.6	3.4	3.3	94.0	-0.6	3.4	3.3	94.0
	Direct-DML (2)	-1.4	6.0	5.2	90.3	8.1	6.6	5.6	89.7	-2.2	3.5	3.3	93.3	1.0	3.8	3.5	93.2	2.0	3.8	3.5	92.0	2.0	3.8	3.5	92.0
	Direct-DML (5)	-4.6	6.4	5.0	87.4	10.3	6.9	5.4	86.6	-3.1	3.5	3.2	92.3	-4.5	3.5	2.3	79.8	-4.5	3.5	2.3	79.8	-4.5	3.5	2.3	79.8
	No-DML	-4.4	5.8	3.8	79.5	-4.3	5.8	3.8	79.6	-4.5	3.5	2.3	79.8	-4.5	3.5	2.3	79.8	-4.5	3.5	2.3	79.8	-4.5	3.5	2.3	79.8
Z_1	Proposed (known)	0.4	5.6	5.5	94.6	0.5	5.7	5.5	94.6	0.1	3.3	3.3	95.0	0.2	3.4	3.3	95.1	0.1	3.4	3.3	95.0	0.1	3.4	3.3	95.0
	Proposed (estimated)	0.5	5.6	5.4	94.6	0.3	5.7	5.5	94.6	0.2	3.3	3.3	95.1	0.1	3.4	3.3	95.0	-3.1	3.7	3.6	93.2	-3.1	3.7	3.6	93.2
	Direct-DML (2)	-5.6	5.9	5.2	89.9	-9.4	6.5	5.6	89.3	-1.4	3.4	3.3	93.4	-5.5	3.8	3.5	92.0	-5.5	3.8	3.5	92.0	-5.5	3.8	3.5	92.0
	Direct-DML (5)	-12.3	6.2	5.0	86.8	-18.7	6.8	5.4	85.5	-3.0	3.5	3.2	92.5	0.0	2.4	2.2	93.6	0.0	2.4	2.2	93.6	0.0	2.4	2.2	93.6
	No-DML	0.0	4.3	3.8	90.7	0.0	4.0	3.8	93.1	0.1	2.6	2.2	90.9	-0.1	3.4	3.3	94.7	-0.1	3.4	3.3	94.7	-0.1	3.4	3.3	94.7
Z_2	Proposed (known)	0.3	5.6	5.5	94.4	0.2	5.7	5.5	94.4	-0.1	3.4	3.3	94.9	-0.1	3.4	3.3	94.7	0.5	3.7	3.6	93.5	0.5	3.7	3.6	93.5
	Proposed (estimated)	0.3	5.6	5.4	94.5	0.4	5.7	5.5	94.4	-0.1	3.4	3.3	94.9	-0.1	3.4	3.3	94.7	-0.1	3.4	3.3	94.7	-0.1	3.4	3.3	94.7
	Direct-DML (2)	-3.0	5.9	5.2	89.9	1.2	6.3	5.6	90.6	-0.9	3.4	3.3	93.3	-2.2	3.5	3.2	92.4	-0.1	3.8	3.5	92.7	-0.1	3.8	3.5	92.7
	Direct-DML (5)	-9.3	6.1	5.0	87.0	-2.0	6.4	5.4	88.8	-2.2	3.5	3.2	92.4	-1.5	4.4	3.8	90.3	-1.5	4.4	3.8	90.3	-1.5	4.4	3.8	90.3
	No-DML	-1.5	4.4	3.8	90.3	-0.9	4.0	3.8	92.8	1.7	2.6	2.2	90.4	1.0	2.4	2.2	93.3	1.0	2.4	2.2	93.3	1.0	2.4	2.2	93.3
X_1	Proposed (known)	0.2	6.3	5.9	92.0	0.2	6.4	6.0	92.0	-0.2	3.7	3.6	93.8	-0.2	3.7	3.6	93.8	-0.2	3.7	3.6	93.8	-0.2	3.7	3.6	93.8
	Proposed (estimated)	0.2	6.3	5.9	92.0	0.2	6.4	6.0	92.0	-0.2	3.7	3.6	93.9	-0.2	3.7	3.6	93.8	-0.2	3.7	3.6	93.8	-0.2	3.7	3.6	93.8
	Direct-DML (2)	-3.4	6.4	5.7	90.6	-4.4	7.0	6.2	90.3	-1.6	3.8	3.6	93.3	-2.1	4.1	3.9	93.3	-2.1	4.1	3.9	93.3	-2.1	4.1	3.9	93.3
	Direct-DML (5)	-7.4	6.6	5.5	88.7	-9.0	7.1	5.9	88.6	-2.9	3.8	3.6	92.4	-3.6	4.1	3.8	92.4	-3.6	4.1	3.8	92.4	-3.6	4.1	3.8	92.4
	No-DML	-3.5	5.7	4.1	83.9	-3.4	5.7	4.1	84.0	-4.4	3.4	2.4	83.6	-4.3	3.4	2.5	83.7	-4.3	3.4	2.5	83.7	-4.3	3.4	2.5	83.7
X_2	Proposed (known)	0.0	6.1	5.8	92.4	0.0	6.2	5.8	92.3	-0.1	3.6	3.5	93.9	-0.1	3.6	3.5	93.9	0.0	3.6	3.5	93.9	0.0	3.6	3.5	93.9
	Proposed (estimated)	0.0	6.1	5.8	92.4	0.0	6.1	5.8	92.3	-0.1	3.6	3.5	93.9	-0.1	3.6	3.5	93.9	0.0	3.6	3.5	93.9	0.0	3.6	3.5	93.9
	Direct-DML (2)	0.5	6.1	5.5	91.4	1.7	6.7	6.0	91.2	0.1	3.6	3.5	93.8	0.7	3.9	3.8	93.6	0.7	3.9	3.8	93.6	0.7	3.9	3.8	93.6
	Direct-DML (5)	0.9	6.2	5.4	90.1	2.8	6.8	5.8	89.8	0.2	3.6	3.4	93.4	0.9	3.9	3.7	93.1	0.9	3.9	3.7	93.1	0.9	3.9	3.7	93.1
	No-DML	0.2	5.5	4.0	84.8	0.2	5.5	4.0	84.9	0.0	3.2	2.4	85.9	0.0	3.2	2.4	85.9	0.0	3.2	2.4	85.9	0.0	3.2	2.4	85.9

(Bias $\times 10^{-3}$): Average bias across all simulation replicates and time points; (SD $\times 10^{-2}$): Average Monte Carlo standard deviation across all time points; (SE $\times 10^{-2}$): Average estimated standard error across all simulation replicates and time points; (CP %): Average coverage probability of the 95% confidence intervals across all time points.

To implement the proposed method, we considered both the case when the delay factor was known (denoted as “Proposed (known)”), and the case when it was estimated as described in Remark 1 (denoted as “Proposed (estimated)”). We compared our method

with two competing approaches. The first method assumed the same delay structure as in Equation (1) but did not use DML as in Equation (3) for estimating the tv-HTEs (i.e., it does not apply centering); this method is denoted as “No-DML”. The second method incorporated DML but disregarded the delay effect structure, that is, it directly modeled $h_{0t}(\mathcal{H}_{it})$ in Equation (5) using some machine learning models (denoted as “Direct-DML”). Incorporating the full history is likely to lead to overfitting, especially when the sample size is small. To mitigate this risk, we assumed that only the current time point and the t_0 most recent time points are used in all ML models. We considered two choices for the memory length t_0 , specifically $t_0 \in \{2, 5\}$, and denote these as Direct-DML (t_0). In Case I, all functions to be estimated are (generalized) linear. Thus, we used the *glmnet* package in *R* (Friedman et al., 2010) to fit the models across all scenarios. In Case II, both the propensity score and baseline outcome functions exhibit a tree structure; accordingly, we use Classification and Regression Trees (CART; Breiman, 1996) across all methods to model these components. For the proposed and No-DML methods, CART is also applied to model the prognostic function. For the Direct-DML methods, we explore various machine learning models (*glmnet*, CART, k-Nearest Neighbors, and Random Forest) using the *caret* package in *R* and fine-tune hyperparameters for optimal performance. Model performance was assessed using four metrics: (i) the average bias of tv-HTEs across all simulation replicates, (ii) the Monte Carlo standard deviation (of the estimated tv-HTEs), (iii) the average estimated standard error, calculated using (8), and (iv) the coverage probabilities of the 95% confidence intervals.

The simulation results based on 500 replicates are presented in Table 1. As shown, the proposed method provides estimates with minimal bias and coverage probabilities close to the nominal 95% level. As the sample size increases, the coverage rate of the proposed

method improves from approximately $92 \sim 93\%$ to around $94 \sim 95\%$, supporting the validity of our theoretical framework. Note that even without knowledge of the true delay factor, the model accurately estimates it, yielding results nearly identical to those obtained when the delay factor is known. In contrast, the No-DML method exhibits notable bias and fails to provide reliable inference, particularly for the intercept tv-HTE. The Direct-DML methods perform better in bias and coverage probabilities over the No-DML method; however, it remains biased and generally falls below the nominal coverage level, especially when $n = 200$ at $t_0 = 5$. This may be due to overfitting of the prognostic function $\delta_t(X_{it}, U_{it})$. Web Figure 1 provides a detailed view of the model performance for the proposed method with a known delay factor in Case I, displaying the average bias and coverage probabilities across all time points. The results indicate that the estimates are unbiased and the inference is accurate across all time points, with increased sample sizes leading to more precise inference.

For Case II, as shown in Table 2, the No-DML method exhibits substantial bias and fails to provide reliable inference, achieving a coverage rate of only around 50% for the intercept tv-HTE when $n = 200$. This issue likely arises from the high correlation between the propensity score and the prognostic function, as discussed in Chernozhukov et al. (2018). In the Direct-DML methods, the limited ability of a single ML model to capture both the nonlinear tree structure of the prognostic function and the linear delayed effects results in higher standard errors for the estimated tv-HTEs. Consequently, this leads to wider confidence intervals and reduced statistical power compared to the proposed method. Overall, the proposed method demonstrates superior performance across all evaluated metrics.

Table 2: Summary of the estimated tv-HTEs across 500 simulations for Case II.

tv-HTE	Method	n = 200								n = 500							
		$\gamma = 0.3$				$\gamma = 0.7$				$\gamma = 0.3$				$\gamma = 0.7$			
		Bias	SD	SE	CP												
Intercept	Proposed (known)	-4.9	6.7	6.6	93.5	-4.8	6.8	6.7	93.5	-2.6	3.8	3.7	93.9	-2.6	3.8	3.7	94.0
	Proposed (estimated)	-5.1	6.6	6.5	93.4	-5.2	6.7	6.6	93.5	-2.6	3.8	3.7	93.9	-2.7	3.8	3.7	94.0
	Direct-DML (2)	-5.4	8.2	7.6	92.1	-1.8	8.6	8.0	92.3	-1.9	4.9	4.8	94.1	-1.1	5.1	5.0	94.2
	Direct-DML (5)	-10.8	8.5	7.5	90.5	-4.1	8.9	7.8	90.6	-3.7	4.9	4.7	93.6	-2.0	5.1	4.9	93.7
	No-DML	-68.7	8.7	4.1	49.4	-70.3	8.6	4.1	48.5	-24.4	4.9	2.4	66.0	-25.4	4.9	2.4	66.0
Z_1	Proposed (known)	-0.4	6.8	6.5	94.8	-0.5	7.0	6.7	94.7	-0.1	3.7	3.6	94.9	0.0	3.7	3.7	94.9
	Proposed (estimated)	-0.4	6.7	6.4	94.8	-0.4	6.9	6.6	94.6	-0.1	3.7	3.6	94.9	-0.1	3.7	3.7	94.9
	Direct-DML (2)	-0.7	8.0	7.6	93.1	-2.4	8.5	8.0	92.7	-0.2	4.8	4.7	94.5	-1.0	5.1	4.9	94.1
	Direct-DML (5)	-1.2	8.1	7.4	92.2	-5.4	8.6	7.7	91.4	-0.4	4.8	4.7	94.3	-2.0	5.1	4.9	93.7
	No-DML	0.0	4.5	4.1	92.1	0.0	4.3	4.1	94.0	-0.1	2.7	2.4	91.2	0.0	2.5	2.4	93.8
Z_2	Proposed (known)	-0.4	6.9	6.6	94.8	-0.4	7.1	6.8	94.7	0.1	3.8	3.7	94.8	0.1	3.8	3.7	94.9
	Proposed (estimated)	-0.5	6.8	6.5	94.7	-0.6	7.0	6.7	94.7	0.0	3.7	3.7	94.8	0.1	3.8	3.7	94.8
	Direct-DML (2)	0.5	8.0	7.6	92.6	2.4	8.5	8.0	92.4	0.3	4.9	4.8	94.1	1.1	5.1	5.0	93.7
	Direct-DML (5)	0.9	8.2	7.4	91.4	5.1	8.6	7.8	90.9	0.5	4.9	4.7	93.9	2.1	5.2	4.9	93.4
	No-DML	-1.2	4.4	4.1	93.2	-0.7	4.3	4.1	94.0	0.6	2.4	2.4	94.5	0.3	2.4	2.4	94.6
X_1	Proposed (known)	0.0	7.5	7.3	94.6	0.2	7.6	7.4	94.5	-2.3	4.1	4.0	94.4	-2.2	4.1	4.1	94.5
	Proposed (estimated)	-0.4	7.3	7.2	94.4	-0.2	7.5	7.3	94.5	-2.4	4.0	4.0	94.5	-2.2	4.1	4.1	94.5
	Direct-DML (2)	-2.1	8.7	8.2	92.2	-2.4	9.1	8.5	92.0	-0.9	5.3	5.1	93.9	-1.2	5.5	5.4	93.8
	Direct-DML (5)	-4.4	8.8	7.9	91.0	-4.8	9.3	8.3	90.8	-1.7	5.3	5.1	93.5	-2.2	5.5	5.3	93.4
	No-DML	-31.8	5.1	4.2	82.2	-24.4	5.0	4.2	86.1	-29.2	3.9	2.4	59.0	-24.3	3.8	2.4	66.4
X_2	Proposed (known)	-0.3	7.4	7.1	94.6	-0.2	7.6	7.3	94.4	0.0	4.1	3.9	94.6	0.0	4.1	4.0	94.6
	Proposed (estimated)	-0.2	7.3	7.0	94.5	-0.2	7.5	7.2	94.5	0.0	4.0	3.9	94.6	-0.1	4.1	4.0	94.6
	Direct-DML (2)	-0.1	8.6	8.1	92.3	0.1	9.1	8.5	92.2	-0.1	5.2	5.1	93.9	0.0	5.5	5.3	93.9
	Direct-DML (5)	-0.2	8.8	8.0	91.3	0.1	9.2	8.3	91.1	-0.1	5.3	5.0	93.5	0.1	5.5	5.3	93.5
	No-DML	0.0	4.7	4.4	93.4	-0.1	4.7	4.4	93.4	0.0	2.7	2.5	93.8	0.0	2.7	2.5	93.7

$(\text{Bias} \times 10^{-3})$: Average bias across all simulation replicates and time points; $(\text{SD} \times 10^{-2})$: Average Monte Carlo standard deviation across all time points; $(\text{SE} \times 10^{-2})$: Average estimated standard error across all simulation replicates and time points; $(\text{CP} \%)$: Average coverage probability of the 95% confidence intervals across all time points.

6 Application

We applied our method to the Mobile Parkinson’s Observatory for Worldwide Evidence-based Research (mPower) study (Bot et al., 2016). The mPower was a six-month longitudinal digital health observational study designed to assess the feasibility of smartphone-based remote monitoring of Parkinson’s disease (PD) symptoms. Its broader objective was to develop digital biomarkers for use in future clinical drug trials. The study included 1,087 participants who self-identified as having a professional PD diagnosis. Among these participants, the majority were taking daily levodopa treatment. While not mandatory, participants were encouraged to complete up to three daily activities throughout the study period. These activities involved five active assessments (tapping, voice, walking, balance,

and memory), during which smartphone sensors recorded relevant data. In the real application, all participants received daily levodopa treatment. For some days, the phenotype of a participant was recorded immediately after levodopa administration so these measurements corresponded to the potential outcomes associated with the medication use ($A_{it} = 1$). For the other days, the phenotype was measured after a significant time had passed since the treatment on the previous day, but before taking medication on the same day; therefore, the outcome was the potential outcome under no medication ($A_{it} = 0$). Moreover, which days to measure phenotypes before or after the medications varied from subject to subject. Comprehensive descriptions of the study design were provided in Bot et al. (2016); Omberg et al. (2022).

In our analysis, we focus mainly on the tapping modality. The tapping assessment evaluates bradykinesia (slowness of movement), which is one of the hallmark symptoms of PD. During the assessment, participants placed the phone on a flat surface and used two fingers from the same hand to alternately tap two fixed points on the screen for 20 seconds. The software recorded both the location and timing of each tap, providing detailed data on tapping speed and rhythm. For our analysis, we used the “mean tapping interval” (i.e., the average time difference between two taps; smaller intervals indicate quicker and better performance) as the outcome variable and applied a logarithmic transformation to address its skewness. We included baseline demographic variables, age, sex, smoking history, years since diagnosis of PD, and deep brain stimulation status (whether a patient has undergone the procedure), to investigate potential heterogeneity in treatment effects based on these factors. Furthermore, we incorporated data from the walking/resting modalities, which assessed participants’ tremors, motor fluctuations, and gait disturbances during walking or standing still. Our aim was to tailor treatment based on global motor control (walk-

ing/resting) to improve the fine motor control of each individual (tapping). This approach could study whether responses to levodopa treatment are consistent in different motor domains. Time-varying walking/resting features assess a participant’s real-time motor function state at specific time points, which can inform personalized treatment adjustments over time. For the walking/resting modality, we used the “median acceleration at resting” as the time-varying tailoring variable, where smaller values indicate better balance while standing still. We used other extracted walking/resting features as additional time-varying prognostic factors. A more detailed definition of these features is available in Xu et al. (2023) and Omberg et al. (2022).

Due to the presence of noisy sensor data, preprocessing was necessary. We followed the preprocessing methods outlined in Xu et al. (2023). Our analysis revealed that most patients had at most one tapping measurement per day. Since the afternoon data were significantly more complete and exhibited different patterns compared to the morning data due to akinesia (Xu et al., 2023; Omberg et al., 2022), we restricted our analysis to only measurements of the afternoon. To ensure data quality, we excluded subjects with excessive missing tapping or walking/resting measurements. After this exclusion, 283 subjects remained in our final analysis. To handle missing time-varying covariates, we used the “*mice*” procedure in R (Van Buuren and Groothuis-Oudshoorn, 2011) for imputation. Specifically, we treated each patient’s digital phenotypes as a cluster, used the day as the random effects, and included both the baseline and time-varying covariates in the imputation. Figure 2 presents the scatterplots of the mean tapping intervals for 20 randomly selected subjects over 50 days by treatment status (treatment status was distinguished using different colors).

We applied our proposed method to analyze the tv-HTEs over the first 50 days. One slight difference was that since the participants received treatment daily, there was a delayed

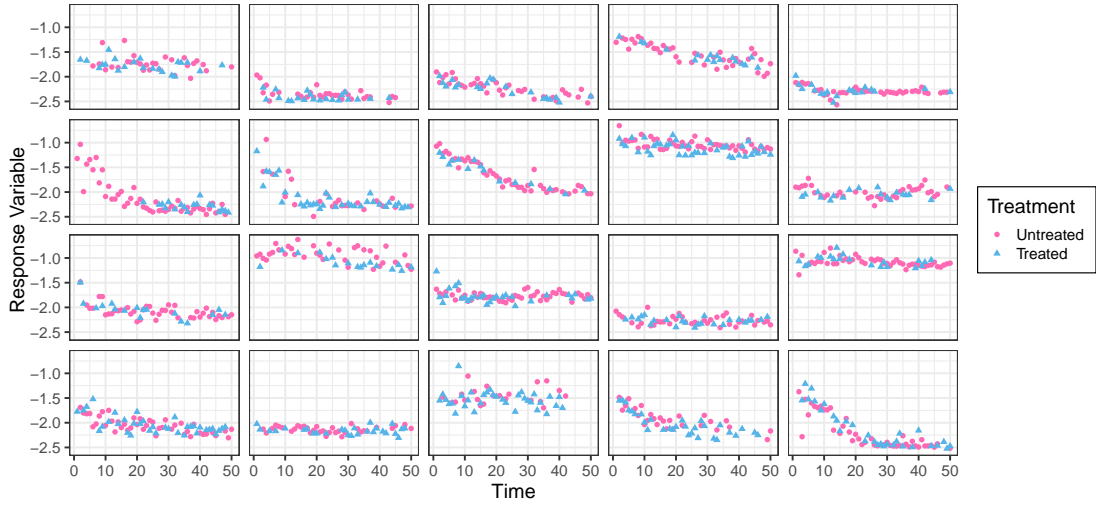


Figure 2: Scatterplot of the response variable (mean tapping intervals) for 20 randomly selected subjects from the mPower data.

effect from each of the past days by time t so in this analysis, $I(A_{is} = 1)$ was removed from the second summation on the right-hand side of equation (1). For this analysis, a negative value of treatment effect indicates an improvement in treatment outcomes, as smaller values of the mean tapping interval represent better fine motor function. Our findings suggested that the treatment was more effective for younger PD patients compared to older patients. Specifically, we dichotomized age at its median for better interpretability (i.e., younger than 60 years of age versus 60 or older). The time-varying treatment effects for these two age groups are presented in Figure 3(a). From the figure, it is evident that there is no consistent treatment effect for patients aged 60 or older, while a clear treatment effect is observed for younger patients. To smooth the time-varying effects, we applied a local smoothing method (Cleveland, 1979) and visualized the mean curve with a 95% confidence band (represented by the shaded area) using “*loess*” in R. The results show an increasing trend in the treatment effect size from day one to day 50.

Furthermore, we examined the effect modification of motor fluctuation at the resting state (where smaller values indicate better balance and gait) on the treatment outcome

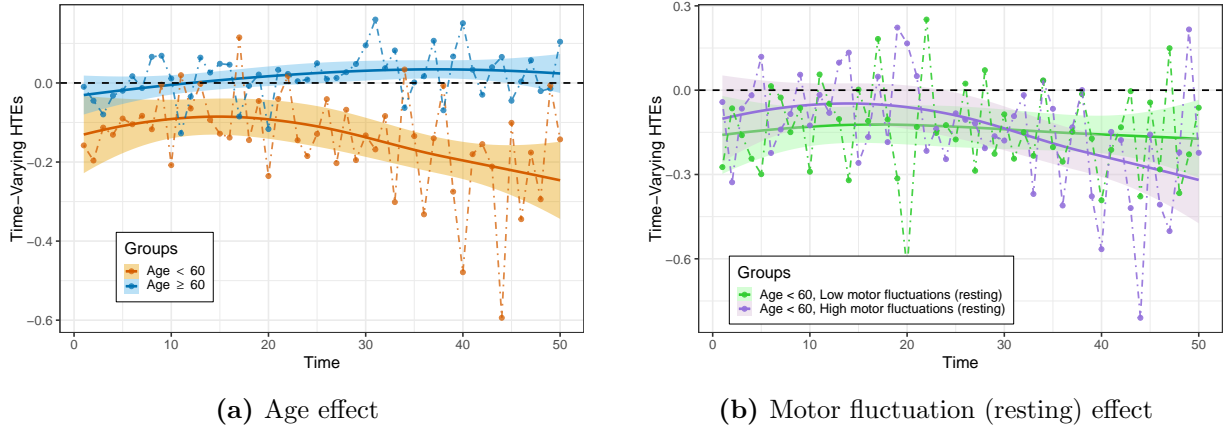
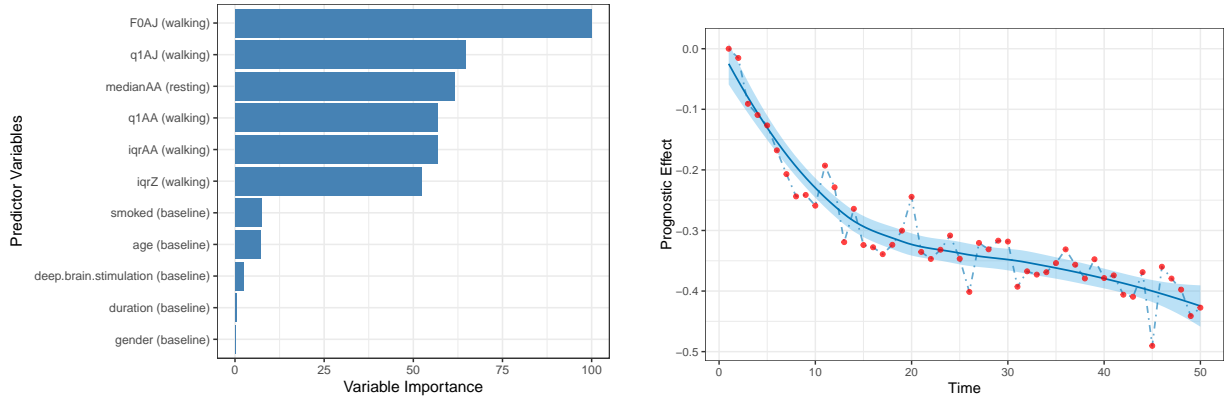


Figure 3: Visualization of time-varying heterogeneous treatment effects using mPower data. Solid dots represent the estimated treatment effects, dashed lines illustrate the time-varying trends, smoothed solid curves show the fitted smoothed trends of the time-varying treatment effects, and shaded areas indicate the 95% confidence bands for the mean estimation.

(tapping). We focused on the younger group (aged under 60) as they showed a significant treatment effect. Specifically, let μ_x and σ_x denote the mean and standard deviation of the median acceleration at resting (computed across all subjects and time points). We present the time-varying treatment effect for low motor fluctuation ($X_{\text{low}} = \mu_x - 2\sigma_x$) and high motor fluctuation ($X_{\text{high}} = \mu_x + 2\sigma_x$) in Figure 3(b). From the smoothed results, we observed that for individuals with low motor fluctuation (i.e., better gait at resting status), the treatment effect was more stable over time compared to those with high motor fluctuation (i.e., worse gait at resting status). In the latter case, the treatment effect begins to manifest after 25 days and gradually increases over time, spanning from 25 to 50 days. By incorporating motor functions as a tailoring variable, we obtain a more refined assessment of personalized treatment effect sizes over time.

For model fitting, we estimated the delay factor as 0.1 using a grid search over the range $\{0, 0.1, \dots, 0.9, 1\}$, minimizing the RMSE. This result suggests that the delay effect in this application is relatively small, which is expected given the short half-life of levodopa medication (Contin and Martinelli, 2010). To estimate the propensity score $\pi_{0t}(\mathcal{H}_{it})$, we



(a) Variable importance for the propensity scores

(b) Prognostic effect over time

Figure 4: Details of the propensity score and prognostic effect models.

trained a Gradient Boosting Machine (GBM) model using the *caret* package in R. The relative importance of variables (Friedman, 2001) is presented in Figure 4(a). Detailed descriptions of each variable can be found at <https://github.com/Sage-Bionetworks/mpowertools/blob/master/FeatureDefinitions.md>. The results suggest that incorporating walking/resting modalities increases the accuracy of the propensity score model. Figure 4(b) illustrates the main prognostic effects over time, revealing a clear decreasing trend. This pattern aligns with the patterns of the outcome variable (tapping intervals) in Figure 2. A possible explanation is that as time progresses, participants become more familiar with the task, leading to improved overall performance similar to a practice effect. This analysis shows that it is important to separate the prognostic effect from the treatment effect.

7 Discussion

In this paper, we proposed a DML method to estimate time-varying delayed and instantaneous treatment effects using digital phenotype data. By decomposing the treatment effect on the outcome into four distinct components (baseline effect, delayed effect, instantaneous

effect, and additional prognostic effect), our approach achieved a more accurate estimation of heterogeneous treatment effects (HTEs) and captures how the treatment effect evolves over time. We used a sequential procedure combined with DML to model both time-varying instantaneous and delayed treatment effects. We proved the asymptotic normality of the proposed estimator, facilitating robust inference. Extensive simulation studies validated the finite-sample performance of our method and demonstrated the advantages of utilizing DML and decomposing treatment effects compared to a regular DML. Applying our approach to the mPower study, we found that the treatment was more effective for younger PD patients than for older ones. Additionally, for individuals with low motor fluctuation, the treatment effect remained more stable over time than for those with high motor fluctuation. We also found a significant prognostic effect consistent with the practice effect. These findings highlight the utility of the proposed method, which separates various sources of treatment manifestation and allows for incorporating time-varying covariates as tailoring variables.

In mHealth studies, causal excursion effect (Boruvka et al., 2018; Qian et al., 2020) measures the impact of a “one-step deviation” from a baseline policy or treatment sequence, capturing the short-term causal effect of an intervention at a given time. These effects are useful for evaluating just-in-time adaptive interventions (JITAIs) in mHealth studies, where treatments are delivered dynamically based on contextual information (e.g., digital phenotypes such as physical activity, mood, or physiological states). Our method can be extended to estimate the causal excursion effect when the treatment administration differs from the observed treatment sequences based on the proposed models. In addition, beyond its application in PD, our proposed method could be applied to track and optimize insulin management in diabetes to maintain glycemic control or monitor walking patterns and

gait stability in older populations, identify early signs of decline, and tailor interventions to maintain mobility and prevent falls.

In Section 4, the Donsker conditions in Condition 3 can be further relaxed by employing data splitting (Chernozhukov et al., 2018). Specifically, we could split the sample into two sets: using the first half to obtain the machine learning estimator and the second half exclusively for estimating the tv-HTEs. This approach allows for the relaxation of the Donsker assumption and permits the use of any complex machine learning estimator as long as it satisfies the order requirements of Condition 3. Data splitting is well known for reducing the risk of overfitting. However, in practice, it often leads to a smaller sample size in each split, resulting in high estimation variance, particularly when the overall sample size is small or there is a significant amount of missing data. Therefore, we opted not to use data splitting in our simulation and data analysis.

Acknowledgements

This research is supported by U.S. National Institutes of Health grants MH123487, NS073671 and GM124104.

Supplementary Materials

Web Appendices and Figures are available with this paper at the Biometrics website on Oxford Academic.

References

Abadie, A., Diamond, A., and Hainmueller, J. (2010). Synthetic control methods for comparative case studies: Estimating the effect of California’s tobacco control program. *Journal of the American Statistical Association*, 105(490):493–505.

Alugubelli, N., Abuissa, H., and Roka, A. (2022). Wearable devices for remote monitoring of heart rate and heart rate variability—what we know and what is coming. *Sensors*, 22(22):8903.

Arkhangelsky, D., Athey, S., Hirshberg, D. A., Imbens, G. W., and Wager, S. (2021). Synthetic difference-in-differences. *American Economic Review*, 111(12):4088–4118.

Bhadtadak, V., Ghewade, B., and Yelne, S. (2024). A comprehensive review on advancements in wearable technologies: Revolutionizing cardiovascular medicine. *Cureus*, 16(5).

Boruvka, A., Almirall, D., Witkiewitz, K., and Murphy, S. A. (2018). Assessing time-varying causal effect moderation in mobile health. *Journal of the American Statistical Association*, 113(523):1112–1121.

Bot, B. M., Suver, C., Neto, E. C., Kellen, M., Klein, A., Bare, C., Doerr, M., Pratap, A., Wilbanks, J., Dorsey, E., et al. (2016). The mPower study, Parkinson disease mobile data collected using ResearchKit. *Scientific Data*, 3(1):1–9.

Breiman, L. (1996). Bagging predictors. *Machine Learning*, 24:123–140.

Callaway, B. and Sant'Anna, P. H. (2021). Difference-in-differences with multiple time periods. *Journal of Econometrics*, 225(2):200–230.

Chernozhukov, V., Chetverikov, D., Demirer, M., Duflo, E., Hansen, C., Newey, W., and Robins, J. (2018). Double/debiased machine learning for treatment and structural parameters. *The Econometrics Journal*, 21(1):C1–C68.

Cleveland, W. S. (1979). Robust locally weighted regression and smoothing scatterplots. *Journal of the American statistical association*, 74(368):829–836.

Contin, M. and Martinelli, P. (2010). Pharmacokinetics of levodopa. *Journal of Neurology*, 257:253–261.

Ding, P. (2024). *A first course in causal inference*. CRC Press.

Friedman, J. H. (2001). Greedy function approximation: A gradient boosting machine. *The Annals of Statistics*, 29(5):1189–1232.

Friedman, J. H., Hastie, T., and Tibshirani, R. (2010). Regularization paths for generalized linear models via coordinate descent. *Journal of Statistical Software*, 33:1–22.

Hatamyar, J., Kreif, N., Rocha, R., and Huber, M. (2023). Machine learning for staggered difference-in-differences and dynamic treatment effect heterogeneity. *arXiv preprint arXiv:2310.11962*.

Hofmann, S. G., Sawyer, A. T., Witt, A. A., and Oh, D. (2010). The effect of mindfulness-based therapy on anxiety and depression: A meta-analytic review. *Journal of consulting and clinical psychology*, 78(2):169.

Horn, R. A. and Johnson, C. R. (2012). *Matrix Analysis*. Cambridge university press.

Jain, S. H., Powers, B. W., Hawkins, J. B., and Brownstein, J. S. (2015). The digital phenotype. *Nature Biotechnology*, 33(5):462–463.

Keus, S., Munneke, M., Graziano, M., Paltamaa, J., Pelosin, E., Domingos, J., Brühlmann, S., Ramaswamy, B., Prins, J., Struiksma, C., et al. (2014). European physiotherapy guideline for parkinson’s disease. *The Netherlands: KNGF/ParkinsonNet*, 191:1–153.

Lewis, G. and Syrgkanis, V. (2021). Double/debiased machine learning for dynamic treatment effects. In *NeurIPS*, pages 22695–22707.

Loh, W. W. and Ren, D. (2023). Estimating time-varying treatment effects in longitudinal

studies. *Psychological Methods*, <https://doi.org/10.1037/met0000574>.

Martinengo, L., Stona, A.-C., Griva, K., Dazzan, P., Pariante, C. M., von Wangenheim,

F., and Car, J. (2021). Self-guided cognitive behavioral therapy apps for depression: systematic assessment of features, functionality, and congruence with evidence. *Journal of medical internet research*, 23(7):e27619.

Nie, X. and Wager, S. (2021). Quasi-oracle estimation of heterogeneous treatment effects.

Biometrika, 108(2):299–319.

Obeso, J. A., Olanow, C. W., and Nutt, J. G. (2000). Levodopa motor complications in

parkinson’s disease. *Trends in neurosciences*, 23:S2–S7.

Omberg, L., Chaibub Neto, E., Perumal, T. M., Pratap, A., Tediarjo, A., Adams, J.,

Bloem, B. R., Bot, B. M., Elson, M., Goldman, S. M., et al. (2022). Remote smartphone monitoring of Parkinson’s disease and individual response to therapy. *Nature Biotechnology*, 40(4):480–487.

Qian, T., Klasnja, P., and Murphy, S. A. (2020). Linear mixed models with endogenous

covariates: modeling sequential treatment effects with application to a mobile health

study. *Statistical Science*, 35(3):375.

Sun, L. and Abraham, S. (2021). Estimating dynamic treatment effects in event studies

with heterogeneous treatment effects. *Journal of Econometrics*, 225(2):175–199.

Vaart, A. W. and Wellner, J. A. (1996). *Weak Convergence and Empirical Processes*.

Springer, New York.

Van Buuren, S. and Groothuis-Oudshoorn, K. (2011). mice: Multivariate imputation by chained equations in r. *Journal of statistical software*, 45:1–67.

Wager, S. and Athey, S. (2018). Estimation and inference of heterogeneous treatment effects using random forests. *Journal of the American Statistical Association*, 113(523):1228–1242.

Willis, A., Schootman, M., Evanoff, B., Perlmutter, J., and Racette, B. (2011). Neurologist care in Parkinson disease: a utilization, outcomes, and survival study. *Neurology*, 77(9):851–857.

Wu, Y., Yao, X., Vespasiani, G., Nicolucci, A., Dong, Y., Kwong, J., Li, L., Sun, X., Tian, H., Li, S., et al. (2017). Mobile app-based interventions to support diabetes self-management: a systematic review of randomized controlled trials to identify functions associated with glycemic efficacy. *JMIR mHealth and uHealth*, 5(3):e6522.

Xu, T., Chen, Y., Zeng, D., and Wang, Y. (2023). Mixed-response state-space model for analyzing multi-dimensional digital phenotypes. *Journal of the American Statistical Association*, 118(544):2288–2300.

Supplementary Materials for “Double Machine Learning for Estimating Time-Varying Delayed and Instantaneous Effects Using Digital Phenotypes”

Xingche Guo, Zexi Cai, Yuanjia Wang, and Donglin Zeng

Web Appendix A

The Web Appendix A contains the proof of theorems. First, note that for the little- o notation, $x_n = o(r_n)$ for $x_n \in \mathbb{R}^d$ means that $a^\top x_n = o_p(r_n)$ for all fixed $a \in \mathbb{R}^d$, and $A_n = o(r_n)$ for $A_n \in \mathbb{R}^{p \times q}$ means that $b^\top \cdot \text{vec}(A_n) = o(r_n)$ for all fixed $b \in \mathbb{R}^{pq}$. It is straightforward to show that if A_n is positive definite, then $A_n = o_p(r_n)$ is equivalent to $\Lambda_{\max}(A_n) = o_p(r_n)$. Similar arguments hold for big- O notation.

Proof of Theorem 1: Define the empirical process $\mathbb{G}_n = n^{1/2} (\mathbb{P}_n - \mathbb{P})$, we have

$$\begin{aligned}
n^{1/2} (\widehat{\beta}_t - \beta_{0t}) &= n^{1/2} \left\{ \widehat{J}_t^{-1} \Psi_t^b (\widehat{\eta}_t) - \beta_{0t} \right\} \\
&= n^{1/2} (J_{0t}^{-1} + R_1) \Psi_t (\beta_{0t}, \widehat{\eta}_t) \\
&= (J_{0t}^{-1} + R_1) \left\{ \mathbb{G}_n S_t(\beta_{0t}, \widehat{\eta}_t) + R_2 \right\} \\
&= (J_{0t}^{-1} + R_1) \left\{ \mathbb{G}_n S_t(\beta_{0t}, \eta_{0t}) + R_2 + R_3 \right\},
\end{aligned}$$

where $R_1 = \widehat{J}_t^{-1} - J_{0t}^{-1}$, $R_2 = n^{1/2} \mathbb{P} S_t(\beta_{0t}, \widehat{\eta}_t)$, $R_3 = \mathbb{G}_n \{ S_t(\beta_{0t}, \widehat{\eta}_t) - S_t(\beta_{0t}, \eta_{0t}) \}$.

To obtain the order of R_1 , we re-express $R_1 = \widehat{J}_t^{-1} (J_{0t} - \widehat{J}_t) J_{0t}^{-1}$. Recall that $J_{0t} =$

$E \left[\pi_{0t}(\mathcal{H}_t) (1 - \pi_{0t}(\mathcal{H}_t)) \tilde{X}_t \tilde{X}_t^\top \right]$. According to Conditions 1 and 2,

$$0 < p_a(1 - p_a)\sigma_{\min}^2 < \Lambda_{\min}(J_{0t}) \leq \Lambda_{\max}(J_{0t}) < \frac{1}{4}\sigma_{\max}^2 < \infty. \quad (\text{S.1})$$

Therefore, $J_{0t}^{-1} = O(1)$. Next, define $S_t^a(\pi_t) = A_t \{A_t - \pi_t(\mathcal{H}_t)\} \tilde{X}_t \tilde{X}_t^\top$. Write

$$\begin{aligned} \hat{J}_t - J_{0t} &= \mathbb{P}_n S_t^a(\hat{\pi}_t) - \mathbb{P} S_t^a(\pi_{0t}) \\ &= n^{-1/2} \mathbb{G}_n S_t^a(\hat{\pi}_t) + \mathbb{P} \{S_t^a(\hat{\pi}_t) - S_t^a(\pi_{0t})\}. \end{aligned}$$

Consider the limiting distribution of $\mathbb{G}_n \text{vec}(S_t^a(\hat{\pi}_t))$. Note that

$$\mathbb{P} \{ \text{vec}(S_t^a(\hat{\pi}_t))^{\otimes 2} \} = \mathbb{P} A_t \{A_t - \hat{\pi}_t(\mathcal{H}_t)\}^2 (\tilde{X}_t \tilde{X}_t^\top) \otimes (\tilde{X}_t \tilde{X}_t^\top).$$

Based on Condition 2 and the requirement that the valid estimate $\hat{\pi}_t(\cdot)$ must lie within the range $[0, 1]$, we can infer that $\Lambda_{\max}(\mathbb{P} \{ \text{vec}(S_t^a(\hat{\pi}_t))^{\otimes 2} \}) \leq \kappa_{\max}^4 < \infty$. Furthermore, according to Condition 3, for any $\hat{\pi}_t \in \mathcal{F}_\pi$, since \mathcal{F}_π is P -Donsker, it follows that $\mathbb{G}_n S_t^a(\hat{\pi}_t) = O_p(1)$. Therefore $n^{-1/2} \mathbb{G}_n S_t^a(\hat{\pi}_t) = O_p(n^{-1/2}) = o_p(1)$. On the other hand, for any fixed $b \in \mathbb{R}^{d^2}$,

$$\begin{aligned} \mathbb{P} \left| b^\top \cdot \text{vec} \{S_t^a(\hat{\pi}_t) - S_t^a(\pi_{0t})\} \right| &= \mathbb{P} \left| A_t \{ \pi_{0t}(\mathcal{H}_t) - \hat{\pi}_t(\mathcal{H}_t) \} b^\top (\tilde{X}_t \otimes \tilde{X}_t) \right| \\ &\leq \kappa_{\max}^2 \|b\|_2 \left[\mathbb{P} \{ \pi_{0t}(\mathcal{H}_t) - \hat{\pi}_t(\mathcal{H}_t) \}^2 \right]^{1/2}. \end{aligned}$$

The inequality follows from the Cauchy-Schwarz inequality. Using Condition 3, we can establish that $\mathbb{P} \{S_t^a(\hat{\pi}_t) - S_t^a(\pi_{0t})\} = o_p(1)$. Consequently, we have $J_{0t} - \hat{J}_t = o_p(1)$.

Finally, according to (Theorem 6.3.2, Horn and Johnson, 2012),

$$\sup_k \left| \Lambda_k(\widehat{J}_t) - \Lambda_k(J_{0t}) \right| \leq \|J_{0t} - \widehat{J}_t\|_2, \quad (\text{S.2})$$

where $\Lambda_k(\cdot)$ indicates the k -th largest eigenvalues for a matrix, $\|\cdot\|_2$ denotes the matrix spectral norm. By (S.1)-(S.2) and the fact that $J_{0t} - \widehat{J}_t = o_p(1)$, we know that with probability one as n tends to infinity, the eigenvalues of \widehat{J}_t lie within the interval $(p_a(1 - p_a)\sigma_{\min}^2 - \epsilon, 4^{-1}\sigma_{\max}^2 + \epsilon)$ for arbitrary small $\epsilon > 0$. Hence $\widehat{J}_t^{-1} = O_p(1)$. Then, we conclude that $\widehat{J}_t^{-1} - J_{0t}^{-1} = o_p(1)$.

To obtain the order of R_2 , according to (6) and the fact that $E[S_t(\beta_{0t}, \eta_{0t})] = 0$,

$$\begin{aligned} |a^\top \cdot R_2| &= n^{1/2} \left| a^\top \cdot \mathbb{P}S_t(\beta_{0t}, \widehat{\eta}_t) \right| \\ &= n^{1/2} \left| \mathbb{P} \left[\left\{ W_t \Delta \widehat{\pi}_t(\mathcal{H}_t) + V_t \Delta \widehat{h}_t(\mathcal{H}_t) + \Delta \widehat{\pi}_t(\mathcal{H}_t) \Delta \widehat{h}_t(\mathcal{H}_t) \right\} \cdot a^\top \widetilde{X}_t \right] \right| \\ &= n^{1/2} \left| \mathbb{P} \left[\Delta \widehat{\pi}_t(\mathcal{H}_t) \Delta \widehat{h}_t(\mathcal{H}_t) \cdot a^\top \widetilde{X}_t \right] \right| \\ &\leq n^{1/2} \mathbb{P} \left| \Delta \widehat{\pi}_t(\mathcal{H}_t) \Delta \widehat{h}_t(\mathcal{H}_t) \cdot a^\top \widetilde{X}_t \right| \\ &\leq n^{1/2} \sigma_{\max} \|a\|_2 \cdot \left[\mathbb{P} \left\{ \Delta \widehat{\pi}_t(\mathcal{H}_t) \Delta \widehat{h}_t(\mathcal{H}_t) \right\}^2 \right]^{1/2} \quad \forall a \in \mathbb{R}^d. \end{aligned}$$

The second equality holds because $E(W_t | \mathcal{H}_t) = 0$ and $E(V_t | \mathcal{H}_t) = 0$. The last inequality follows from the Cauchy-Schwarz inequality. By Condition 3, we conclude that $R_2 = o_p(1)$.

For R_3 , we first note that $S_t(\beta_{0t}, \widehat{\eta}_t) - S_t(\beta_{0t}, \eta_{0t}) = Q_{1,t} + Q_{2,t}$, where

$$Q_{1,t} = W_t \Delta \widehat{\pi}_t(\mathcal{H}_t) \widetilde{X}_t \quad \text{and} \quad Q_{2,t} = \left\{ (V_t + \Delta \widehat{\pi}_t(\mathcal{H}_t)) \Delta \widehat{h}_t(\mathcal{H}_t) \right\} \widetilde{X}_t.$$

Next, we note that for all fixed $b \in \mathbb{R}^{d^2}$,

$$\begin{aligned}
\left| b^\top \cdot \mathbb{P} \{Q_{1,t} \otimes Q_{1,t}\} \right| &= \left| \mathbb{P} W_t^2 \{\Delta \widehat{\pi}_t(\mathcal{H}_t)\}^2 \cdot b^\top (\widetilde{X}_t \otimes \widetilde{X}_t) \right| \\
&\leq \mathbb{P} \left\{ E (W_t^2 \mid \mathcal{H}_t) \{\Delta \widehat{\pi}_t(\mathcal{H}_t)\}^2 \cdot \left| b^\top (\widetilde{X}_t \otimes \widetilde{X}_t) \right| \right\} \\
&\leq c \cdot \mathbb{P} \left\{ \{\Delta \widehat{\pi}_t(\mathcal{H}_t)\}^2 \cdot \left| b^\top (\widetilde{X}_t \otimes \widetilde{X}_t) \right| \right\} \\
&\leq c \kappa_{\max}^2 \|b\|_2 \cdot [\mathbb{P} \{\Delta \widehat{\pi}_t(\mathcal{H}_t)\}^4]^{1/2}. \tag{S.3}
\end{aligned}$$

Similarly, note that $V_t \in [-1, 1]$, $\Delta \widehat{\pi}_t(\mathcal{H}_t) \in [-1, 1]$, then

$$\begin{aligned}
\left| b^\top \cdot \mathbb{P} \{Q_{2,t} \otimes Q_{2,t}\} \right| &\leq \mathbb{P} \left[\left\{ (V_t + \Delta \widehat{\pi}_t(\mathcal{H}_t)) \Delta \widehat{h}_t(\mathcal{H}_t) \right\}^2 \cdot \left| b^\top (\widetilde{X}_t \otimes \widetilde{X}_t) \right| \right] \\
&\leq 4 \kappa_{\max}^2 \|b\|_2 \cdot \left[\mathbb{P} \left\{ \Delta \widehat{h}_t(\mathcal{H}_t) \right\}^4 \right]^{1/2}. \tag{S.4}
\end{aligned}$$

According to Condition 3, both (S.3) and (S.4) are of order $o_p(1)$. Furthermore, because \mathcal{F}_π and \mathcal{F}_{h_t} are both P -Donsker, $\mathbb{G}_n Q_{1,t}$ and $\mathbb{G}_n Q_{2,t}$ converge in distribution to zero-mean Gaussian distributions with covariance matrices $\mathbb{P} Q_{1,t}^{\otimes 2}$ and $\mathbb{P} Q_{2,t}^{\otimes 2}$, respectively. As a result, $R_3 = \mathbb{G}_n Q_{1,t} + \mathbb{G}_n Q_{2,t} = O_p(1) \cdot o_p(1) = o_p(1)$.

Finally, combining these results, we obtain

$$n^{1/2} \left(\widehat{\beta}_t - \beta_{0t} \right) = J_{0t}^{-1} \mathbb{G}_n S_t(\beta_{0t}, \eta_{0t}) + o_p(1).$$

Thus, by the Central Limit Theorem, we conclude $n^{1/2} \left(\widehat{\beta}_t - \beta_{0t} \right) \xrightarrow{d} N(0, \Psi_0)$. \square

Proof of Theorem 2: The proof follows the same arguments as the above proof to obtain

$$\begin{aligned}
n^{1/2} (\widehat{\beta}_t - \beta_{0t}) &= n^{1/2} \left\{ \widehat{J}_t^{-1} \Psi_t^b(\widehat{\eta}_t) - \beta_{0t} \right\} \\
&= n^{1/2} (J_{0t}^{-1} + R_1) \Psi_t(\beta_{0t}, \widehat{\eta}_t) \\
&= (J_{0t}^{-1} + R_1(t)) \left\{ \mathbb{G}_n S_t(\beta_{0t}, \widehat{\eta}_t) + R_2(t) \right\} \\
&= (J_{0t}^{-1} + R_1(t)) \left\{ \mathbb{G}_n S_t(\beta_{0t}, \eta_{0t}) + R_2(t) + R_3(t) \right\},
\end{aligned}$$

where $R_1(t) = \widehat{J}_t^{-1} - J_{0t}^{-1}$, $R_2(t) = n^{1/2} \mathbb{P} S_t(\beta_{0t}, \widehat{\eta}_t)$, $R_3(t) = \mathbb{G}_n \{S_t(\beta_{0t}, \widehat{\eta}_t) - S_t(\beta_{0t}, \eta_{0t})\}$.

Note that $R_1(t)$ and $R_2(t)$ are $o_p(1)$ uniformly in t for $t = 1, \dots, T$ because of the uniform convergence of $\widehat{\pi}_t$ and $\widehat{\delta}_t$ in Condition 3 and the Donsker property of $S_t(\beta_{0t}, \widehat{\eta}_t)$. Since A_t, Y_t and \widetilde{X}_t are the realization of some random processes that have bounded total variations and Condition 3 holds, both $Q_{1,t}$ and $Q_{2,t}$ as a function of t belong to some Donsker class so $R_3(t) = \sqrt{n} O_p(\sup_t \|\widehat{\eta}_t - \eta_{0t}\|^2)$. Therefore, we obtain

$$\sup_t \left| n^{1/2} (\widehat{\beta}_t - \beta_{0t}) - J_{0t}^{-1} \mathbb{G}_n S_t(\beta_{0t}, \eta_{0t}) \right| = o_p(1).$$

Equivalently, it gives

$$\sup_{s \in \{1/T, 2/T, \dots\}} \left| n^{1/2} (\widehat{\xi}(s) - \xi_0(s)) - \mathbb{G}_n \widetilde{\Gamma}(s) \right| = o_p(1).$$

Therefore, by the definition of $\widehat{\xi}$ and the continuous differentiability of ξ_0 , we have

$$\begin{aligned}
& \sup_{s \in [0,1]} \left| n^{1/2} \left(\widehat{\xi}(s) - \xi_0(s) \right) - \mathbb{G}_n \widetilde{\Gamma}(s) \right| \\
& \leq \sup_{s \in \{1/T, 2/T, \dots\}} \left| n^{1/2} \left(\widehat{\xi}(s) - \xi_0(s) \right) - \mathbb{G}_n \widetilde{\Gamma}(s) \right| \\
& \quad + \sup_{t=1, \dots, T} \sup_{s \in [(t-1)/T, t/T]} \left\{ \sqrt{n} |\xi_0(s) - \xi_0(t/T)| + \left| \mathbb{G}_n \left(\widetilde{\Gamma}(s) - \widetilde{\Gamma}(t/T) \right) \right| \right\} \\
& \leq \sup_{t=1, \dots, T} \sup_{s \in [(t-1)/T, t/T]} \left| \mathbb{G}_n \left(\widetilde{\Gamma}(s) - \widetilde{\Gamma}(t/T) \right) \right| + o_p(1) + O(\sqrt{n}/T).
\end{aligned}$$

Theorem 2 follows from the fact that $\sqrt{n}/T \rightarrow 0$ and the pointwise convergence of the covariance function for $\widetilde{\Gamma}(s)$ to the continuous function $\widetilde{\Sigma}_0$. \square

Web Appendix B

The Web Appendix B contains additional Figures for the simulation studies.

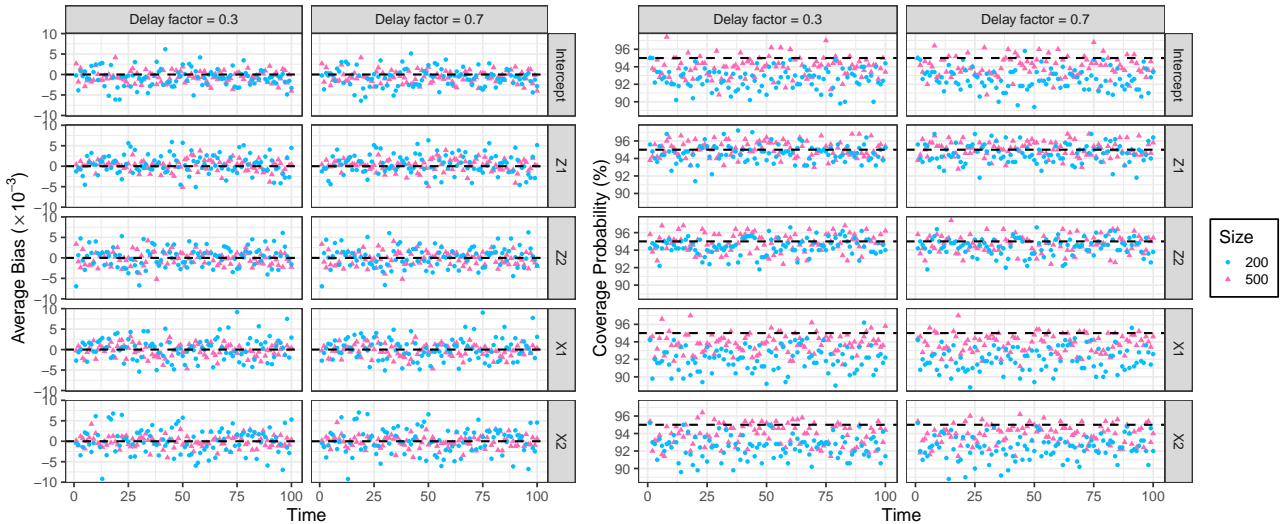


Figure S.1: Performance of the proposed method (with known delay factor) over time across 500 simulations for Case I. The left panel shows the average bias, and the right panel displays the coverage probabilities.